ELSEVIER

Chemical Engineering Journal 136 (2008) 398–408

Chemical Engineering Journal

www.elsevier.com/locate/cej

Synthesis of α-Ni(OH)$_2$ with hydrotalcite-like structure: Precursor for the formation of NiO and Ni nanomaterials with fibrous shapes

Yong Li [a], Xiaowei Xie [a], Junlong Liu [a], Mei Cai [b], Jerry Rogers [b], Wenjie Shen [a,*]

[a] *State Key Laboratory of Catalysis, Dalian Institute of Chemical Physics, Chinese Academy of Sciences, Dalian 116023, China*
[b] *GM Research & Development Center, Warren, MI 48090-9055, USA*

Received 5 April 2007; received in revised form 22 May 2007; accepted 1 June 2007

Abstract

α-Ni(OH)$_2$ with hydrotalcite-like structure was prepared by precipitation of nickel acetate and sodium carbonate aqueous solution with the mediation of ethylene glycol at 393 K. Thermal calcination of this nickel hydroxide precursor at 573–1073 K resulted in the formation of fibrous nickel oxides with diameter of 4–8 nm and length of several hundreds of nanometers. Further reduction of these NiO samples with hydrogen at 773 K led to the formation of metallic Ni with fibrous-like morphology. Most promisingly, these novel nanostructured Ni materials showed much higher catalytic activities not only for the decomposition of methane to hydrogen and carbon nanofibers, but also for the hydrogenation reactions of unsaturated organic compounds.

Keywords: α-Ni(OH)$_2$; Ethylene glycol; Fibrous shape; Nickel oxide; Metallic Ni

1. Introduction

Nanosized nickel materials with controllable morphologies are expected to show interesting chemical and physical properties for the potential applications in catalysis, electronic and magnetic fields [1]. Nickel hydroxide has been regarded as the most important intermediate during the synthesis of nickel oxide and metallic nickel in liquid phase. Nickel hydroxide often exhibits a hexagonal layered structure with two polymorphs, known as α- and β-forms [2]. The layers are well ordered and closely packed in the β-phase of nickel hydroxide with the interlayer distance of ca. 4.6 Å, but they are randomly arranged with water and anionic species as intercalated in the α-phase. Therefore, the interlayer distance of α-Ni(OH)$_2$ is much more dependent on the sizes of the anionic species. Considerable efforts have been devoted to understand the structural features and electrochemical properties of nickel hydroxide during charge–recharge recycle in alkaline secondary batteries [3–6], but little attention was paid to the usage of nickel hydroxide to produce nanosized nickel oxides and/or metallic nickel as potential catalysts.

Thermal calcination of β-Ni(OH)$_2$ often results in the formation of spherical NiO particles, and the particle size is critically dependent on the calcination temperature. Lower temperature calcination (<573 K) gave the particle sizes of NiO less than 10 nm, while very large particles more than 20 nm were produced once the calcination was performed at relatively higher temperatures (>773 K) [7]. Recently, β-Ni(OH)$_2$ in the forms of nanorods [8], nanosheets [9], nanoribbons [10], nanotubes [11], pancakes [12] and hollow spheres [13,14] have been successfully prepared in liquid phase. Further calcination of those β-Ni(OH)$_2$ precursors led to the formation of nickel oxides with various structural features. For instance, NiO nanorings were produced by calcination of Ni(OH)$_2$ nanorods at 773 K [8], and NiO nanosheets were prepared by thermal decomposition of β-Ni(OH)$_2$ nanosheets at 673 K [9]. Obviously, the morphologies of the nickel oxides strongly depended on the shapes of the β-Ni(OH)$_2$ precursors.

On the other hand, it is rather difficult to get stable α-Ni(OH)$_2$ with hydrotalcite-like structures in liquid phase, since it rapidly turned into β-Ni(OH)$_2$ [2]. Precipitation of nickel salts with liquid ammonia [15], cathodic reduction of nickel nitrate [16], homogeneous urea hydrolysis of nickel nitrate [17,18], and sonochemical synthesis [19] have been proposed to be effective routes for preparing stable α-Ni(OH)$_2$. However, there still lacks of mild and fast chemical route to synthesis stable α-nickel

* Corresponding author. Tel.: +86 411 84379085; fax: +86 411 84694447.
E-mail address: shen98@dicp.ac.cn (W. Shen).

1385-8947/$ – see front matter © 2007 Elsevier B.V. All rights reserved.
doi:10.1016/j.cej.2007.06.001

hydroxide in liquid phase. Because of this, decomposition α-$Ni(OH)_2$ for producing nanosized NiO materials with controlled morphologies has not been reported so far.

Ethylene glycol (EG) was previously used to prepare nanostructured noble metals (Pt, Pd, Rh, etc.), and the role of ethylene glycol was attributed to reduce the metal cations and to stabilize the formed metal particles [20,21]. Nanoscaled metal oxides, such as $CoAl_2O_4$, Cr_2O_3, CeO_2, TiO_2 and Fe_2O_3, were also prepared in the solution of diethylene glycol (DEG) [22–24]. Under these circumstances, the polyalcohols acted as a stabilizer, inhibiting the growth and agglomeration of the formed particles. Hydrolysis in polyol (DEG and EG) also provides an effective way to prepare layered double hydroxide [25]. The polyalcohols participate in the formation of metal alkoxides, which may play a significant role in determining the mobility and stability of metal cations and consequently the mechanism of inorganic polymerization [26].

We have recently found that the precipitation media and temperature could significantly influence the structure of the nickel hydroxide precipitate, and consequently the particle size as well as the shape of the nickel oxides [27]. Precipitation in water only resulted in spherical NiO particles, while precipitation in ethylene glycol could give spherical, fibrous and nanorods of NiO, depending on the precipitation temperature. Among them, the fibrous NiO showed extremely high catalytic activity and stability for methane decomposition to produce CO-free hydrogen and carbon nanofibers. In the present work, we extend to study the formation mechanism and the structure features of the stable α-$Ni(OH)_2$ with hydrotalcite-like structure by precipitation of nickel acetate and sodium carbonate aqueous solution in the presence of ethylene glycol at 393 K, and the fibrous NiO and Ni nanomaterials produced by the subsequent thermal calcination and hydrogen reduction of the nickel hydroxide precursor. Moreover, we evaluate the catalytic performance of the Ni nanomaterials, which showed much higher catalytic activities not only for methane decomposition reaction, but also for hydrogenation reactions of unsaturated organic compounds.

2. Experimental

2.1. Preparation of materials

The nickel hydroxide was prepared by precipitation of nickel acetate dissolved in ethylene glycol with sodium carbonate aqueous solution at 393 K. A solution containing 0.05 mol of nickel acetate ($Ni(OAc)_2{\cdot}4H_2O$) and 150 mL of ethylene glycol (EG) was gradually heated to 393 K under stirring and maintained at this temperature for 30 min. Then, 500 mL of 0.2 M Na_2CO_3 aqueous solutions was slowly added into the Ni–EG mixture at 393 K. The precipitate was further aged in the mother liquid for 1 h. After filtration and thoroughly washing with distilled water, the obtained solid was dried at 373 K overnight. The nickel oxides were then obtained by thermal calcination of the nickel hydroxide in air at 573–1073 K for 4 h. Further reduction of the NiO samples with hydrogen at 773 K resulted in the formation of metallic nickel.

For comparison, a reference NiO sample was also prepared by precipitation of nickel acetate dissolved in water with sodium carbonate aqueous solution at 353 K. The precipitate was thoroughly washed with distilled water and dried at 373 K overnight, followed by thermal calcination at 673 K for 4 h in air.

2.2. Characterization

Nitrogen adsorption–desorption isotherms of the nickel oxides were performed using a Nova 4200e (Quantachrome) system operated at 77 K. Prior to measurement, the sample was degassed by vacuum at 573 K for 5 h. The BET surface area was calculated from a multipoint Brunauer–Emmett–Teller analysis of the nitrogen adsorption isotherms.

X-ray powder diffraction (XRD) patterns were recorded on a D/MAX 2500 X-ray diffractometer (Rigaku), using Cu Kα radiation operated at 40 kV and 100 mA. In situ XRD measurements of the reduction of NiO samples with hydrogen were performed in a high temperature chamber installed in the diffractometer. The NiO was pressed into flake and mounted in the chamber where the nickel oxides were reduced with pure hydrogen at 573–973 K for 1h. The mean crystallite sizes of nickel and NiO were calculated from the Scherrer equation.

HRTEM images were taken on Philips Tecnai $G^2$20 operated at 200 kV. Specimens were prepared by ultrasonically suspending the sample in ethanol. A drop of the suspension was then applied onto clean holy copper grids and dried in air.

Scanning electron microscopy images were obtained with a Philips Fei Quanta 200F FEG-SEM.

Thermal Gravimetry and Differential Thermal Analysis (TG-DTA) of the nickel hydroxide was measured on the Pyris Diamond of Perkin-Elmer.

FT-IR spectra were obtained by transmission on a Bruker Vector 22 spectrometer with pressed KBr pellets in the range of 400–4000 cm^{-1} with 4 cm^{-1} resolution.

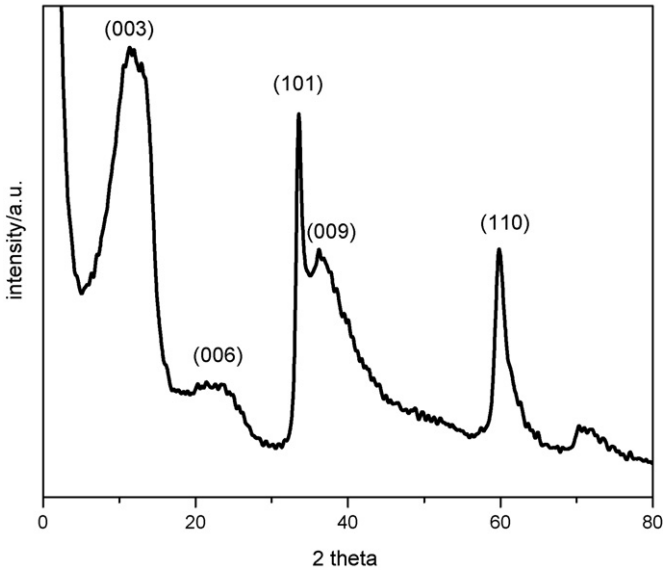

Fig. 1. XRD pattern of the nickel hydroxide precipitate.

Temperature-programmed reduction (TPR) of nickel oxides was performed in a conventional setup equipped with a TCD detector. 50 mg NiO were loaded and heated to 673 K (10 K/min) under N_2 flow (40 mL/min) to remove the adsorbed carbonates and hydrates. After cooling down to room temperature and introducing the reduction agent of 20 vol% H_2/N_2 (40 mL/min), the temperature was then programmed to rise at a ramp of 10 K/min from 303 K to 1073 K.

2.3. Catalytic tests

Methane decomposition reaction ($CH_4 \rightarrow C + 2H_2$) was conducted with a continuous flow fixed-bed quartz reactor (internal diameter of 28 mm) at 773 K under atmospheric pressure. 40 mg NiO sample was loaded and prereduced into metallic Ni with pure hydrogen (20 mL/min) at 773 K for 1 h. The Ni catalyst was flushed with Ar for 0.5 h, pure CH_4 (30–60 mL/min) was

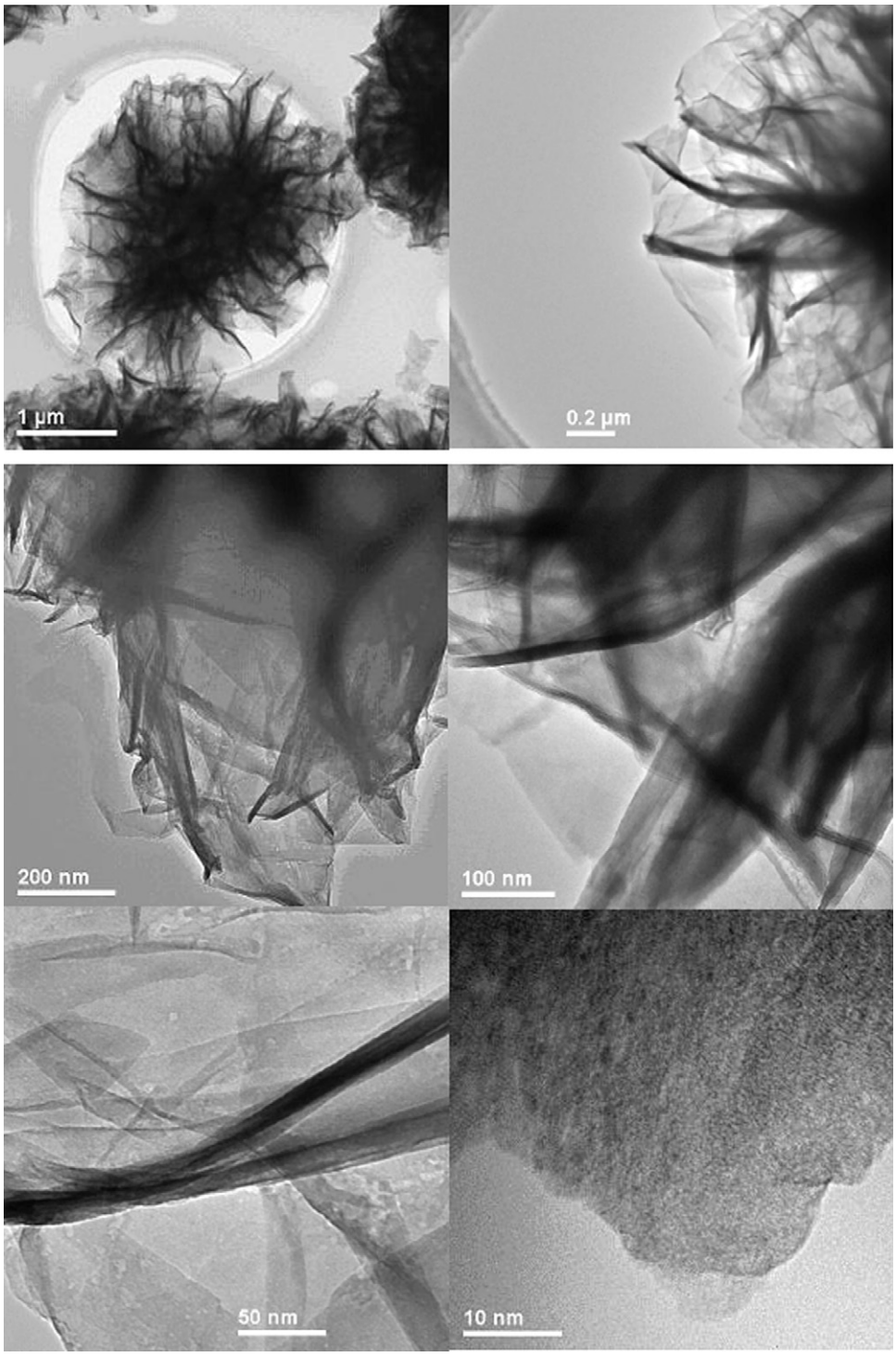

Fig. 2. HRTEM images of the nickel hydroxide precipitate.

then introduced through a mass-flow controller. The effluents from the reactor were analyzed by online gas chromatography. The amount of carbon deposited on the catalyst was determined by weighing the samples, through which the carbon capacity, i.e. grams of carbon deposited per-gram of nickel (g C/g Ni), was calculated.

Hydrogenation reaction of unsaturated organic compounds was carried out with a conventional gas-flow fixed-bed reactor system (internal diameter of 6 mm). 100 mg NiO was reduced into metallic Ni by hydrogen at 773 K for 1 h and flushed with Ar. The unsaturated organic substrate was injected by a syringe pump and the hydrogen was introduced through a mass-flow controller. The effluents from the reactor were analyzed by online gas chromatography.

3. Results and discussion

3.1. Structural characterization of α-nickel hydroxide

Fig. 1 shows the XRD pattern of the as-prepared nickel hydroxide. Clearly, this precipitate exhibited characteristic diffractions of α-$Ni(OH)_2$ (JCPDS #38–0715), which is isostructural with hydrotalcite-like compounds [2]. No diffraction peaks due to β-$Ni(OH)_2$ (JCPDS #14–0117) could be observed. The typical peaks at about $d = 7.56$, 3.78, 2.66, and 1.54 Å can be assigned to the (0 0 3), (0 0 6), (1 0 1) and (1 1 0) planes, respectively, indicating the formation of pure α-$Ni(OH)_2$ [15–19]. The α-type nickel hydroxide generally consisted of a stacking of positively charged $Ni(OH)_{2-x}$ layers with intercalated ions, such as NO_3^-, CO_3^{2-}, CH_3COO^-, and $(CH_2)_4(COO)^{2-}$ to restore its charge neutrality [15–19,28]. The interlayer distance, which was usually calculated from the (0 0 3) plane, was found to depend on the nature of the counter-ion contained in the mother solution. The α-$Ni(OH)_2$ containing CH_3COO^- as intercalated ions has an interlayer distance of ca. 9.4 Å, while the α-$Ni(OH)_2$ containing intercalated NO_3^- and CO_3^{2-} ions has an interlayer distance of ca. 7.6 Å [28,29]. The as-prepared α-$Ni(OH)_2$ only has a interlayer distance of 7.56 Å, implying that the intercalated species is CO_3^{2-}, not CH_3COO^-. Since the hydroxide slabs lose their orientation due to the presence of interleaving water layers, α-type nickel hydroxides are often poorly ordered and exhibit broad bands in their X-ray diffraction patterns [2]. The asymmetric nature of the (1 0 1) plane indicated the formation of a turbostratic phase as observed in most of the previously reported α-$Ni(OH)_2$ materials [2,15–19]. Fig. 2 gives the HRTEM images of the α-$Ni(OH)_2$ precipitate. It exhibited the characteristic features of turbostratic materials, appearing as aggregates of thin crumpled sheets without definite shape, in good accordance with previous observations [2–28].

Fig. 3 shows the IR spectrum of the nickel hydroxide. The narrow band at 3644 cm^{-1} was attributed to the free hydroxyl groups, and the broad band at 3600–3400 cm^{-1} represented the hydroxyl groups and water molecules, which were extensively hydrogen bonded [2,15–19]. The highly basic media may account for the presence of structural hydroxyl groups. The peak around 1654 cm^{-1} was due to the bending vibration of the

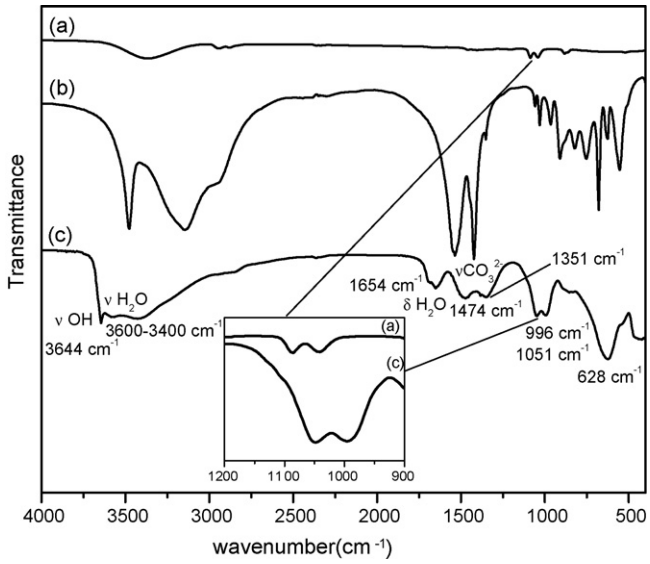

Fig. 3. FT-IR spectra of (a) ethylene glycol, (b) $Ni(OAc)_2{\cdot}4H_2O$ and (c) the as-prepared α-$Ni(OH)_2$.

interlayer water molecules, which is more pronounced in the turbostratic hydroxide. Characteristic bands due to the unidentate carbonate anions were present at 1474 and 1351 cm^{-1} [30]. However, the possible presence of acetate cannot be ruled out, because the characteristic bands of acetate maybe shadowed or overlapped at 1600–1300 cm^{-1}. Together with the XRD data, it can be speculated that these acetate species might be adsorbed on the external surface of the crystallinities. The intensive peaks at 1051 and 996 cm^{-1} corresponded to stretching vibrations of (C–C–O) in ethylene glycol with a clear shift to lower wavenumber, compared to pure ethylene glycol bands. At low wavenumbers, two bands appearing at 623 and 480 cm^{-1} represented the δOH and ν(Ni–O) vibrations, respectively [15–19].

Layered double hydroxides (LDHs) have been extensively investigated as host materials for a range of anion exchange intercalation reactions [31,32]. Ethylene glycol, with the nominal diameter of 4.2 Å, has been thought to be grafted into kaolinite [33], boehmite [34], gibbsite [35], and Zn-Al double hydroxide [36], by measuring the variation of the interlayer distances. Meanwhile, the infrared spectra with clear shift or splitting were also observed compared to pure ethylene glycol. More recently, Mg-Al hydrotalcite containing two grafted components—ethylene glycol and CO_3^{2-} groups with the interlayer distance of 7.4 Å were successfully prepared [37]. By considering the interlayer distance of 7.56 Å for the current α-$Ni(OH)_2$ together with the FTIR observation, it can be assumed that both ethylene glycol and CO_3^{2-} group were all intercalated into the nickel hydroxide layer. The significant shift of the intensive peaks representing the vibrations of (C–C–O) in ethylene glycol to 1051 and 996 cm^{-1} further evidenced that the ethylene glycol might be chemically bonded to the nickel hydroxide layers. This is quite different from the previously reported layered Ni-Al and Co-Al double hydroxides [25], which were prepared by hydrolysis in the solution of diethylene glycol (DEG) or ethylene glycol (EG). Although the characteristic absorption bands of polyols (DEG and EG) around 1100 cm^{-1} were observed,

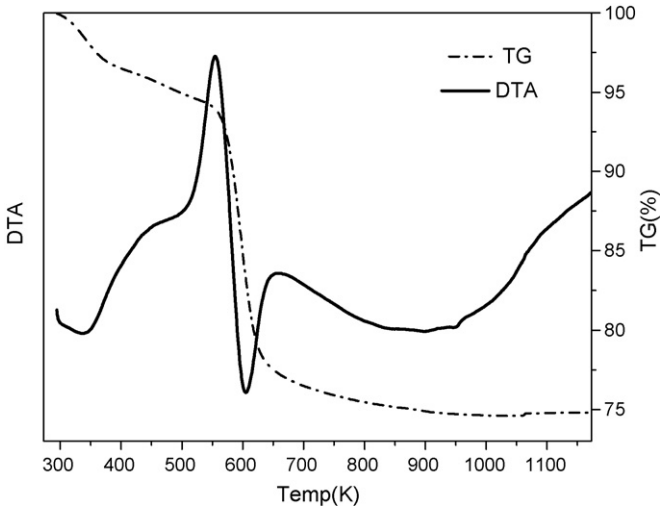

Fig. 4. TG-DTA profile of the as-prepared α-Ni(OH)$_2$.

there were no any shift or splitting in the spectra, implying that the polyalcohols might be only physically adsorbed on the crystal surface as neutral species [25–38].

Fig. 4 illustrates the TG-DTA profile of the nickel hydroxide precipitate. Obviously, the α-Ni(OH)$_2$ underwent multi-step weight losses due to dehydration and decomposition. The initial weight loss of about 3% with a broad endothermic peak at 303–380 K represented the removal of the physically adsorbed water molecules. The followed weight loss of about 20% between 380 and 555 K with a broad and strong exothermic peak corresponded to the departure of the intercalated water molecules and the combustion of ethylene glycol. This combustion with a strong exothermic effect was probably caused by a catalytic oxidation of ethylene glycol with the presence of the generated nickel oxide [38]. Beyond 555 K, all the intercalated water molecules and organic species were completely removed from the interslab space, leading to the destruction of the Ni(OH)$_2$ sheet and the simultaneous formation of NiO.

3.2. Nickel oxides obtained by thermal calcination of the α-Ni(OH)$_2$

Fig. 5 shows the XRD patterns of the nickel oxides obtained by thermal calcination of the nickel hydroxide precipitate in the temperature range of 573–1073 K. Obviously, the NiO samples exhibited typical face-centered cubic structure of nickel oxide (JCPDS #4-835), regardless of calcination temperature. The half-widths of the diffraction peaks of nickel oxides were gradually becoming narrower with increasing temperature, indicating the growth of NiO crystallines. With increasing the calcination temperature from 573 to 1073 K, the crystallite size of NiO only increased from 3.0 to 8.1 nm and the surface area slightly decreased from 147 to 79 $m^2\,g^{-1}$. Nitrogen adsorption–desorption isothermals of the nickel oxides exhibited H3-type hysteresis loop in the IUPAC classifications, indicating aggregates of plate-like particles. This is particularly true for the lamellar hydrotalcite-like materials which present this type of microtexture [39].

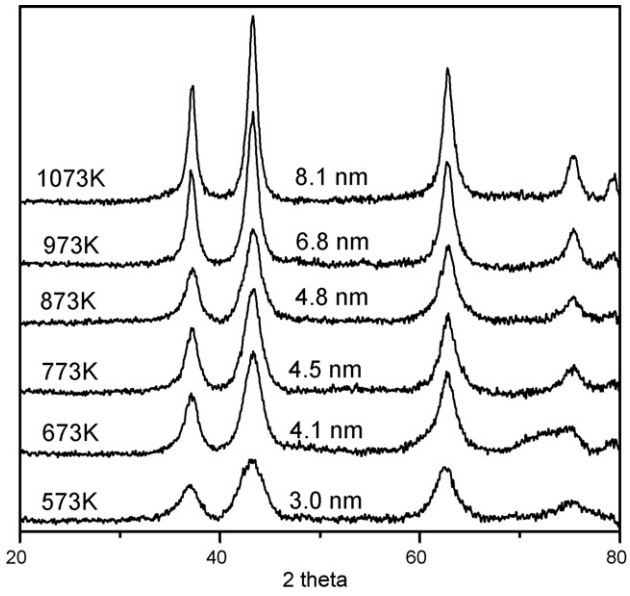

Fig. 5. XRD patterns of the NiO samples by calcination of the α-Ni(OH)$_2$. The crystalline size of NiO was calculated from the main diffraction peak at $2\theta = 43.2^\circ$.

Fig. 6 gives the HRTEM images of the nickel oxides. It can be seen that the interlayered structure of α-Ni(OH)$_2$ precursor still remained in the nickel oxides even after calcination at 1073 K, and the bundles turned to be shorter with increasing calcination temperature. Fig. 7 further shows the characteristic fibrous shapes of the NiO materials obtained by thermal calcination of nickel hydroxide at 673 K. Clearly, the length of the fibrous NiO approached to several hundreds of nanometers and the width was only ca.4 nm. The SEM images of the NiO materials presented in Fig. 8 demonstrate the typical morphology of platelet-like shapes with an unordered crystallite aggregation. These observations are quite promising for NiO materials, since the previously reported nickel oxides often showed spherical shapes and relatively weak thermal stability. A careful survey of the previous studies on NiO materials may find that the obtained spherical NiO particles were small size (<10 nm) with a high surface area only after low temperature calcinations (≤673 K), while very large nanoparticles (>20 nm) were produced once the calcination was performed at relatively higher temperatures (≥973 K) [40,41]. Up to date, there is little work on the preparation of NiO nanostructures with high temperature stability and non-spherical morphology. Thus, the present study achieved not only the rather small crystalline size of NiO even at high temperature, but also the most interesting fibrous shapes from the nickel hydroxide precipitate to the nickel oxides.

3.3. Metallic Ni obtained by hydrogen reduction of NiO

Since metallic nickel is general regarded as the active component in the heterogeneous catalysis with nickel-based materials, the NiO sample obtained by calcination of the α-Ni(OH)$_2$ was further reduced with hydrogen to obtain metallic Ni. Fig. 9 compares the H_2-TPR profiles of the fibrous NiO obtained by calcination of the α-Ni(OH)$_2$ at 673 K and the reference NiO

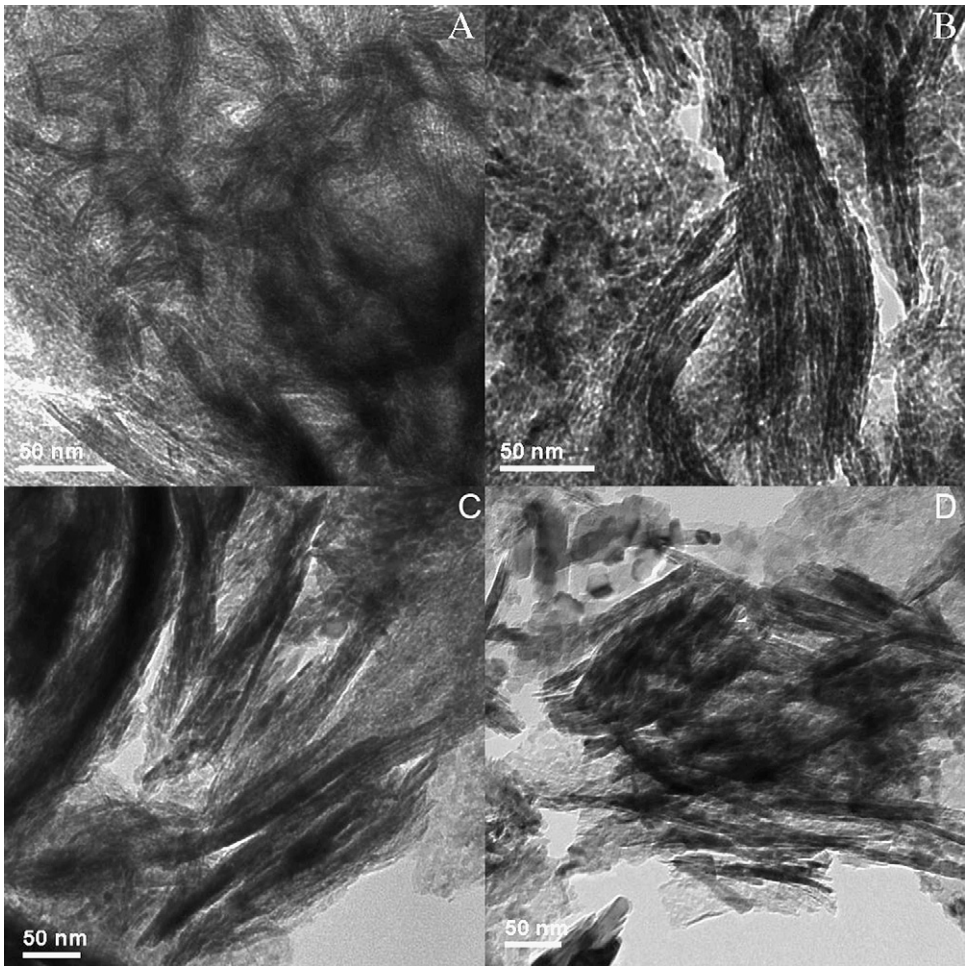

Fig. 6. HRTEM images of the NiO samples by calcination of the as-prepared α-$Ni(OH)_2$. (A) 573 K; (B) 773 K; (C) 973 K; (D) 1073 K.

sample with conventional spherical shapes [27]. It is clear that there is a strong and sharp hydrogen consumption peak appeared at around 600 K for the reference NiO, representing the characteristic reduction of typical nickel oxide particles. However, the fibrous NiO exhibited a relatively broaden hydrogen consumption peak at higher temperature (675 K). Although the amounts of consumed hydrogen calculated from the TPR profiles were about 13–14 mmol H_2/g NiO, indicating that the NiO samples in both cases were completely reduced into metallic nickel, the difference in reduction temperature suggested that the morphology of NiO might greatly influence the reduction behavior. Fig. 10 further shows the XRD patterns for the reduction of this fibrous NiO. The metallic nickel phase appeared at 573 K and the diffraction peaks of NiO almost vanished at 673 K, suggesting that NiO was completely converted to metallic nickel with crystalline size of 7.2 nm. With further increasing the reduction temperature, the diffractions of metallic Ni were gradually becoming extensive and sharper, indicating the enlarging of metallic Ni crystallines. The crystalline size of nickel increased to 12 nm at 873 K and then it was rapidly aggregated into large crystallines of 24 nm when the reduction was performed at 973 K. However, it should be noted that these crystalline sizes are still rather small when compared with conventional spherical Ni particles under such high temperature and reductive atmosphere. It was previously stated that the reduction temperature of NiO increased with increasing the particle size of NiO in the range of 6–17 nm [7], but there are few reports on the effect of morphology on the reduction behavior of NiO. For the current fibrous NiO, the calculated crystalline size of NiO was only 4.1 nm, and it should be practically and easily reduced into metallic Ni at lower temperatures. However, its reduction was completed at higher temperature than the reference NiO sample (crystalline size of 8.4 nm). Therefore, it is reasonable to speculate that the interlayered structure of the fibrous NiO sample hindered the reduction of NiO. As a matter of fact, H_2-TPD studies of a Ni/SiO_2 catalyst have already revealed that the morphology can indeed influence the desorption features of metallic nickel, and the nickel in whisker shapes are more reactive towards hydrogen than spherical nickel [42]. Therefore, the interlayered fibrous structure of the current NiO may greatly influence the reduction features, resulting in significant difference in the TPR profiles when compared with conventional spherical NiO particles.

More importantly, the fibrous-like morphology still remained in the metallic Ni materials, as demonstrated by HRTEM observations shown in Fig. 11. There only presented metallic Ni with fibrous shape and no spherical Ni particles could be observed. This finding of rather stable fibrous shapes from α-$Ni(OH)_2$ and nickel oxide precursors to metallic nickel is quite interest-

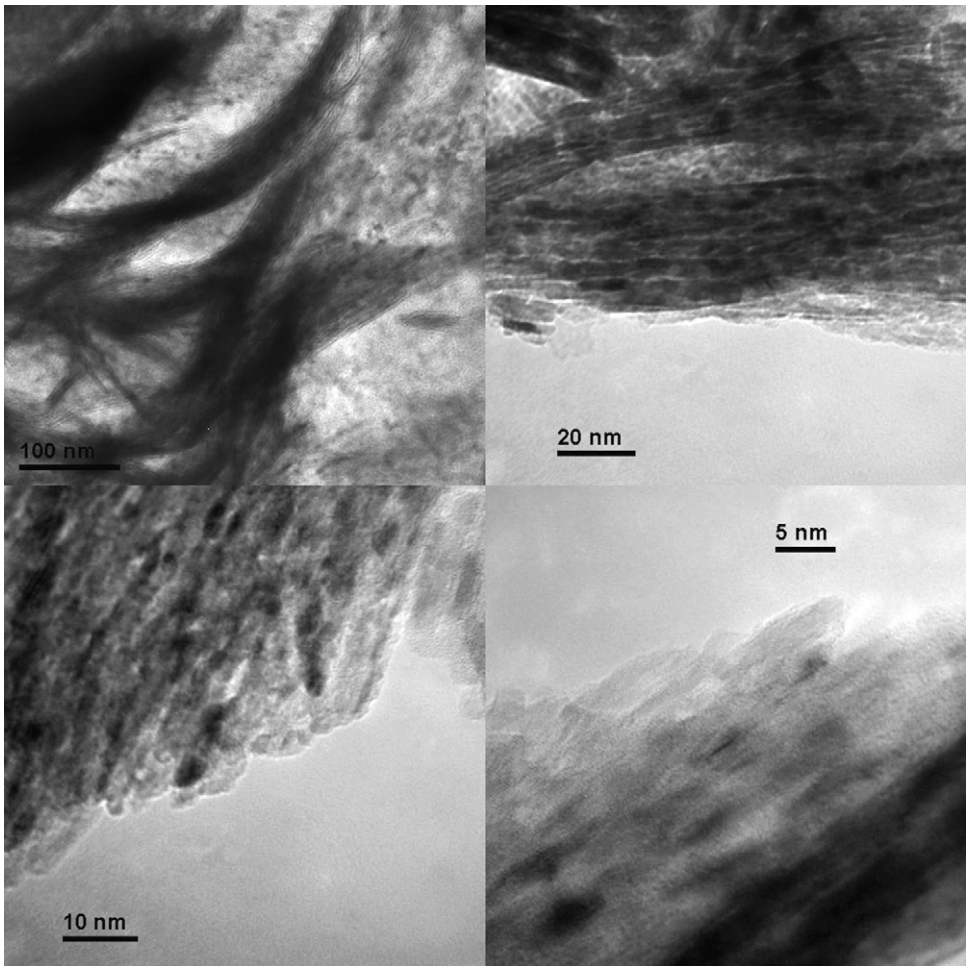

Fig. 7. HRTEM images of the NiO sample obtained by thermal calcination of the α-$Ni(OH)_2$ at 673 K.

ing for nanostructured NiO and Ni materials, because the nickel nanomaterials with unique morphologies were mainly generated from β-$Ni(OH)_2$ precursors in previous studies [8–14]. Only whisker-like morphology of metallic nickel supported by SiO_2 was synthesized by carefully control of the reduction step, and this structure could only be achieved with much lower nickel loading (<2%) and the surface area of silica must be less than 15 $m^2\ g^{-1}$ [42]. Although there were many reports on the preparation of nanosized metallic nickel materials with controlled morphologies using different methods, to our knowledge, the NiO and Ni with the same fibrous-like shapes has not been reported so far.

3.4. Catalytic performance of the fibrous Ni materials

Catalytic decomposition of methane has recently received increasing attention as a potentially economical route to produce CO-free hydrogen for fuel cell applications, and Ni catalysts were demonstrated to be much active for this reaction [43–46]. We have recently reported that the Ni catalysts obtained from the fibrous nickel oxides by hydrogen reduction could show much higher catalytic activities for methane cracking, compared with conventional spherical Ni particles [27]. When the crystalline size of NiO increased from 3.0 to 8.1 nm, the carbon yield only altered in the range of 354–394 g C/g Ni, and the corresponding hydrogen yield slightly varied between 3463 and 3854 mol H_2/mol Ni. It was interestingly found that the NiO materials with crystalline size of 3–8.1 nm were reduced into fibrous Ni with crystalline size of 9–11 nm, and thus explained the similar catalytic activities of the novel metallic nickel for methane decomposition. Here we further demonstrated that the carbon yield over the novel Ni catalyst could increase to 498 g C/g Ni with the hydrogen yield of 4814 mol H_2/mol Ni by decreasing the methane flow rate to 30 mL/min, as shown in Fig. 12. This result is very similar to the highest carbon yield of 491 g C/g Ni, which was obtained over the most effective 40% Ni/SiO_2 catalyst [43].

The most important factor that influences the carbon yield during methane decomposition is the particle size of metallic nickel, and thus great efforts have been paid to disperse and to stabilize the nickel particles with appropriate supporting materials [44–46]. In principle, the use of a catalyst containing only metallic Ni phase without the presence of any support would give sufficient carbon storage capacity on a per-gram basis of the catalyst, but the easy aggregation and sintering of nickel particles under high operation temperatures required to use metal oxides as support for keeping the thermal stability of the dispersed Ni particles. Little attention was paid to use nickel hydroxide

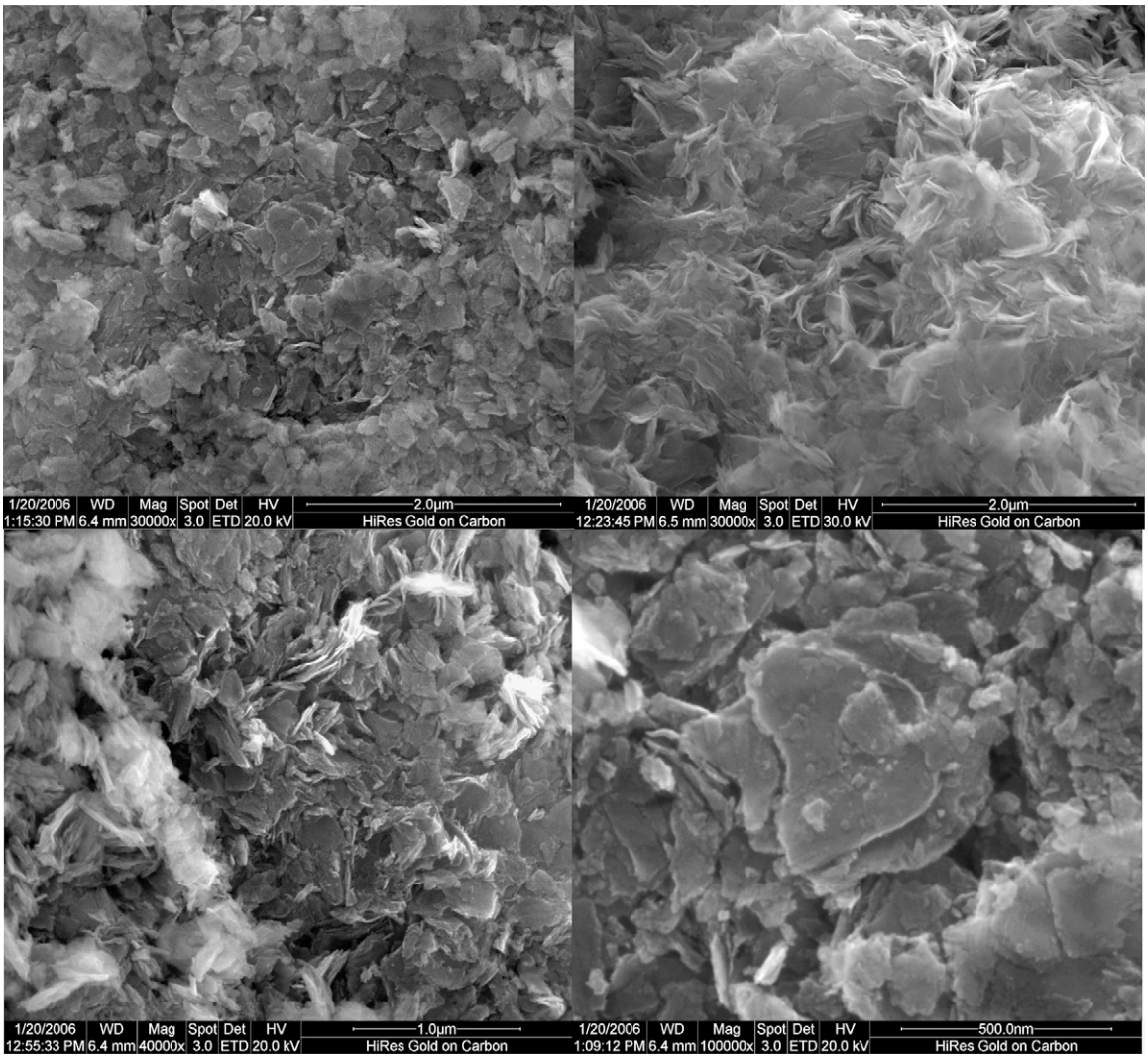

Fig. 8. FE-SEM images of the NiO sample obtained by thermal calcination of the α-$Ni(OH)_2$ at 673 K.

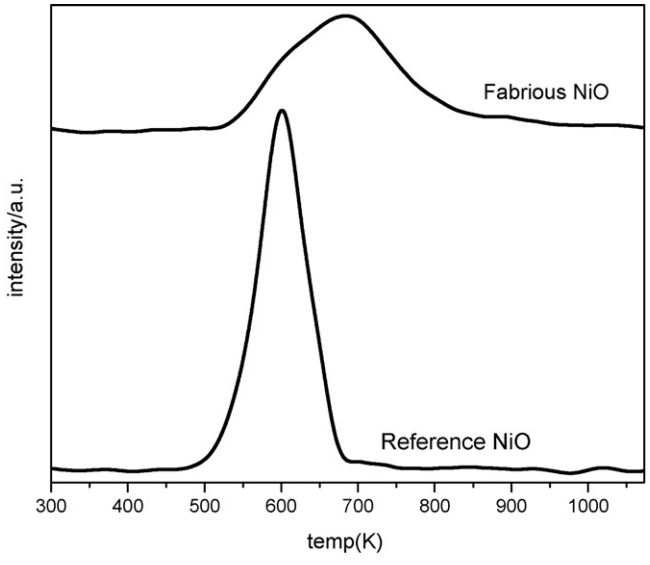

Fig. 9. TPR profiles of the fibrous NiO and the reference NiO.

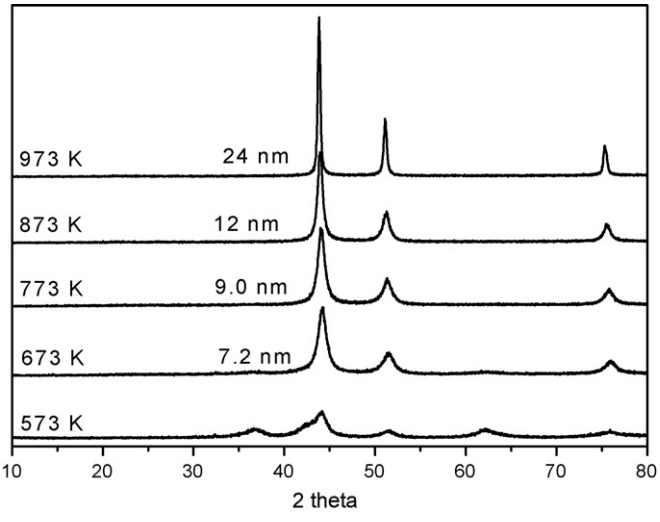

Fig. 10. XRD patterns of the nickel oxide during hydrogen reduction process. The crystalline size of Ni was calculated from the diffraction peak at $2\theta = 45.8^\circ$.

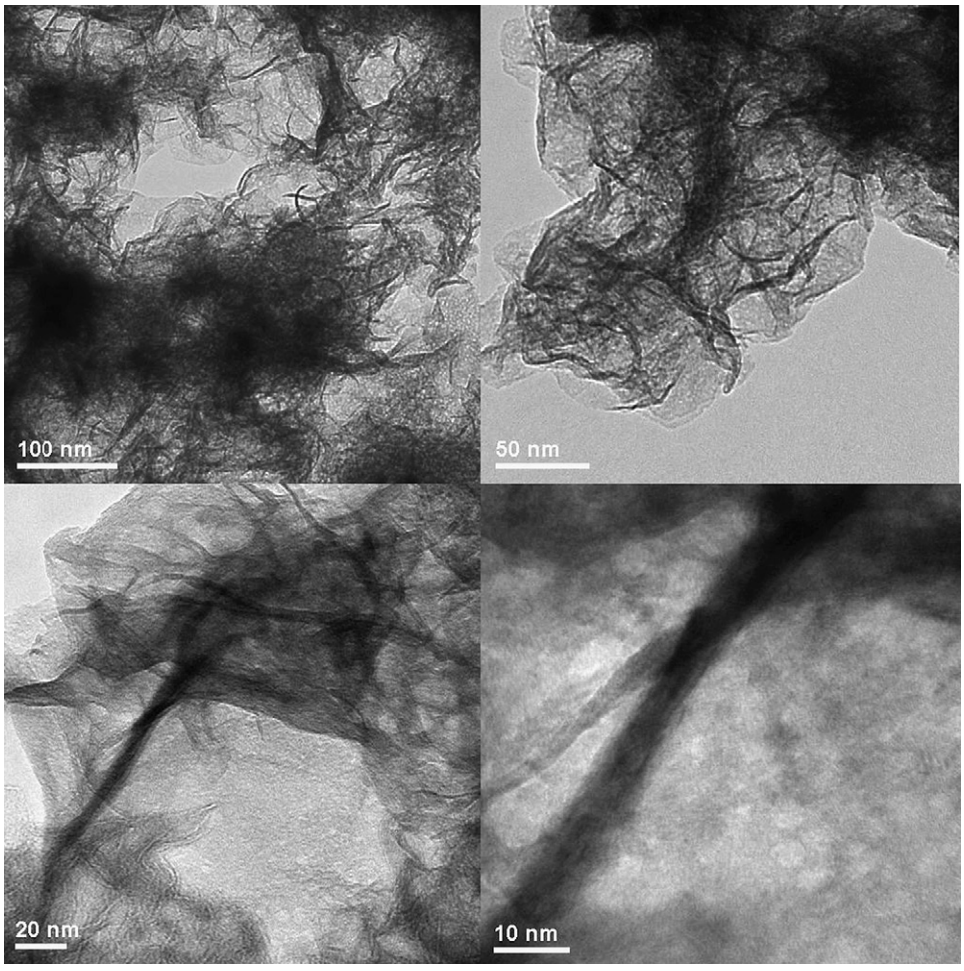

Fig. 11. HRTEM images of metallic Ni produced by hydrogen reduction of NiO at 773 K.

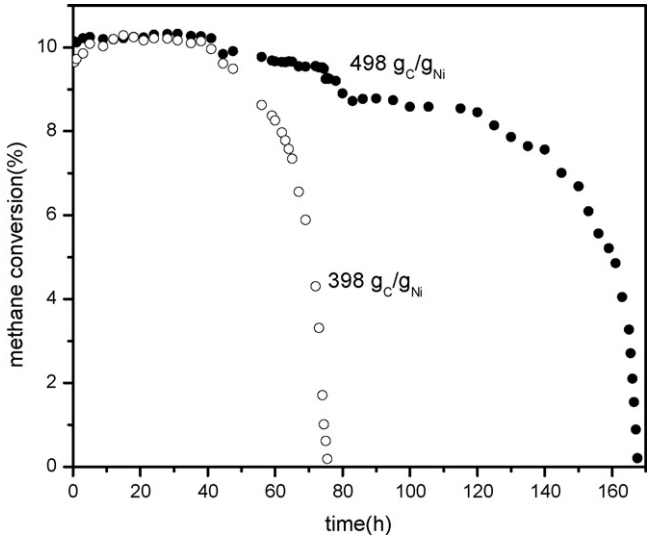

Fig. 12. Methane conversion as a function of time-on-stream over the Ni catalyst. Reaction temperature, 773 K, catalyst, 0.040 g NiO, methane flow rate, 30–60 mL/min.

as precursors to prepare unsupported nickel catalyst. In addition to show the much high activity and durability for methane decomposition, the fibrous Ni also could provide another advantage to the easy removal of catalyst components for the carbon nanofibers.

The NiO sample obtained by calcination of α-$Ni(OH)_2$ with hydrotalcite-like structures at 673 K was further reduced into metallic Ni with hydrogen at 773 K. The resulting Ni catalyst was then employed for gas-phase hydrogenation of unsaturated organic compounds in a continuous flow fixed-bed reactor at atmospheric pressure. As shown in Table 1, the Ni catalyst showed extremely higher activity and selectivity not only in the hydrogenation of benzene and acetone, which are two model substrates of hydrogenation, but also in the hydrogenation of nitrobenzene to aniline and phenol to cyclohexanol. Moreover, the Ni catalyst also exhibited rather high catalytic durability, as illustrated in Fig. 13. Currently, the hydrogenations of unsaturated organic compounds are mainly conducted in autoclave model using Raney Ni catalysts under severe conditions [47]. For example, hydrogenation of benzene to cyclohexane is carried out at 493 K and 4.0 MPa of H_2 [48]. Whereas, the fibrous Ni catalyst could give 100% conversion of benzene at 373 K under atmospheric pressure in continuous flow operation. Phenol hydrogenation to cyclohexanol is industrially performed at

Table 1
Hydrogenation test of different substrates using the fibrous Ni catalyst

Substrate	Reaction temperature (K)	Selectivity (%)	Conversion (%)
Benzene	373	Cyclohexane ~100	>99.5
Acetone	373	Isopropanol ~100	>95
Nitrobenzene[a]	373	Aniline ~90	>99
Phenol[b]	473	Cyclohexanol ~88 Cyclohexanone ~12	>99

Reaction conditions: H_2, 20 mL/min; liquid feed rate, 0.00667 mL/min, 100 mg NiO prereduced with hydrogen at 673 K.
[a] $C_6H_5NO_2$:C_6H_{12} = 1:1 (vol).
[b] C_6H_5OH:C_6H_{12} = 1:4 (wt).

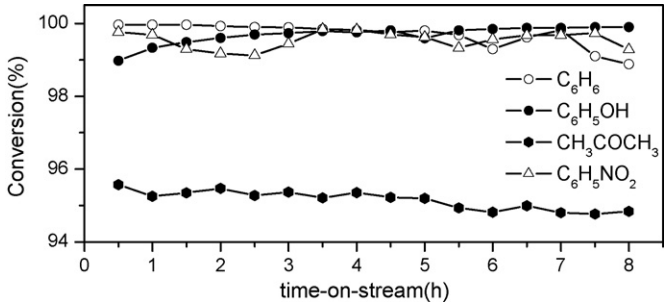

Fig. 13. Hydrogenation reactions of unsaturated organic substrates over the fibrous Ni catalyst.

373 K and 13–15 MPa of H_2 by using Raney Ni [48], but the current continuous flow operation using the fibrous Ni catalyst gives 100% conversion of phenol and 88% selectivity of cyclohexanol at 473 K even under atmospheric pressure of hydrogen. Obviously, this novel nanostructured Ni catalyst generated from α-$Ni(OH)_2$ and NiO precursors showed rather high catalytic performance in hydrogenation of these organic substrates under much mild operation conditions. Another important superiority of this fibrous Ni catalyst over the Raney Ni lies in the environmental begin feature of its preparation. Raney Ni catalysts, which are still very much in use today for a variety of large industrial hydrogenation processes, are traditionally produced by the removal of aluminum from a Ni/Al alloy with a strong alkaline solution. This kind of preparation process does not meet the up-to-date requirements of resources saving by considering the leaching of aluminum from binary alloys, the heavy pollution of alumina-rich alkaline wastes, and the operating safety due to inflammable.

4. Conclusion

α-$Ni(OH)_2$ with hydrotalcite-like structures have been successfully prepared in liquid phase with the mediation of ethylene glycol. Thermal calcination of this nickel hydroxide precursor resulted in the formation NiO nanomaterials with interlayered structures. Such a solution phase approach provided a more promising route for preparing size and morphology-controlled NiO nanomaterials. Further reduction of the NiO with hydrogen led to the formation of fibrous metallic nickel catalysts, which showed extremely high catalytic activities towards hydrogenations of organic substrates and methane cracking reaction.

References

[1] C. Burda, X.B. Chen, R. Narayanan, M.A. El-Sayed, Chem. Rev. 105 (2005) 1025.
[2] P. Oliva, J. Leonardi, J.F. Laurent, C. Delmas, J.F. Braconnier, M. Figlarz, F. Fievet, A. De Guibert, J. Power Sources 8 (1982) 229.
[3] H.B. Liu, L. Xiang, Y. Jin, Cryst. Growth Des. 6 (2006) 283.
[4] W.K. Hu, D. Noréus, Chem. Mater. 15 (2003) 974.
[5] X.Y. Wang, H. Luo, P.V. Parkhutik, A.-c. Millan, E. Matveeva, J. Power Sources 115 (2003) 153.
[6] F. Bardé, M.P. Palacin, Y. Chabre, O. Isnard, J.M. Tarascon, Chem. Mater. 16 (2004) 3936.
[7] C.B. Wang, G.Y. Gan, S.J. Gau, C.W. Tang, J.L. Bi, Catal. Lett. 101 (2005) 241.
[8] J.H. Liang, Y.D. Li, Chem. Lett. 32 (2003) 1126.
[9] Z.H. Liang, Y.J. Zhu, X.L. Hu, J. Phys. Chem. B 108 (2004) 3488.
[10] D.N. Yang, R.M. Wang, M.S. He, J. Zhang, Z.F. Liu, J. Phys. Chem. B 109 (2005) 7654.
[11] F.S. Cai, G.Y. Zhang, J. Chen, X.L. Gou, H.K. Liu, S.X. Dou, Angew. Chem. Int. Ed. 43 (2004) 4212.
[12] C. Coudun, J.F. Hochepied, J. Phys. Chem. B 109 (2005) 6069.
[13] D.B. Wang, C.X. Song, Z.S. Hu, X. Fu, J. Phys. Chem. B 109 (2005) 1125.
[14] Y. Wang, Q.S. Zhu, H.G. Zhang, Chem. Commun. (2005) 5231.
[15] P. Genin, A. Delahaye-Vidal, F. Portemer, K. Tekaia-Elhsissen, M. Figlarz, Eur. J. Solid State Inorg. Chem. 28 (1991) 505.
[16] K.C. Ho, J. Jorne, J. Electrochem. Soc. 137 (1990) 149.
[17] G.J. de, A. Soler-Illia, A.E. Regazzoni, M.A. Blesa, Chem. Mater. 11 (1999) 3140.
[18] M. Jayalakshmi, N. Venugopal, B.R. Reddy, R.M. Mohan, J. Power Sources 150 (2005) 272.
[19] P. Jeevanandam, Y. Koltypin, A. Gedanken, Nano. Lett. 1 (2001) 263.
[20] C. Bock, C. Paquet, M. Couillard, G.A. Botton, B.R. Macdougall, J. Am. Chem. Soc. 126 (2004) 8028.
[21] S.H. Im, Y.T. Lee, B. Wiley, Y.N. Xia, Angew. Chem. Int. Ed. 44 (2005) 2154.
[22] C. Merikhi, H.O. Jungk, C. Feldmann, J. Mater. Chem. 10 (2000) 1311.
[23] C. Feldmann, H.O. Jungk, Angew. Chem. Int. Ed. 40 (2001) 359.
[24] C. Feldmann, Adv. Funct. Mater. 13 (2003) 101.
[25] V. Prevot, C. Forano, J.P. Besse, Chem. Mater. 17 (2005) 6695.
[26] D. Larcher, G. Sudant, R. Patrice, J.M. Tarascon, Chem. Mater. 15 (2003) 3543.
[27] Y. Li, B.C. Zhang, X.W. Xie, J.L. Liu, Y.D. Xu, W.J. Shen, J. Catal. 238 (2006) 412.
[28] A. Delahaye-Vidal, B. Beaudoin, N. Sac-Epée, K. Tekaia-Elhsissen, A. Audemer, M. Figlarz, Solid State Ionics 84 (1996) 239.
[29] H. Nishizawa, T. Kishikawa, H. Minami, J. Solid State Chem. 146 (1999) 39.
[30] C. Faure, Y. Borthomieu, C. Delmas, M. Fouassier, J. Power Sources 36 (1991) 113.
[31] A.I. Khan, D. O'Hare, J. Mater. Chem. 12 (2002) 3191.
[32] V. Rives, Mater. Chem. Phys. 75 (2002) 19.
[33] J. Tunney, C. Detelier, Clays Clay Miner. 42 (1994) 473.
[34] M. Inoue, H. Kominami, Y. Kondo, T. Inui, Chem. Mater. 9 (1997) 1614.

[35] M. Inoue, Y. Kondo, T. Inui, Inorg. Chem. 27 (1988) 215.
[36] J.L. Guimarães, R. Marangoni, L.P. Ramos, F. Wypych, J. Colloid Interface Sci. 227 (2000) 445.
[37] T. Stanimirova, T. Hibino, Appl. Clay Sci. 31 (2006) 65.
[38] L. Poul, N. Jouini, F. Fiėvet, Chem. Mater. 12 (2000) 3123.
[39] D. Tichit, S. Ribet, B. Coq, Eur. J. Inorg. Chem. (2001) 539.
[40] B. Xia, I.W. Lenggoro, K. Okuyama, Chem. Mater. 14 (2002) 2623.
[41] N.R. Jana, Y.F. Chen, X.G. Peng, Chem. Mater. 16 (2004) 3931.
[42] A.G. Boudjahem, S. Monteverdi, M. Mercy, M.M. Bettahar, J. Catal. 221 (2004) 325.
[43] T.V. Choudhary, C. Sivadinarayana, C.C. Chusuei, A. Klinghoffer, D.W. Goodman, J. Catal. 199 (2001) 9.
[44] S. Takenaka, S. Kobayashi, H. Ogihara, K. Otsuka, J. Catal. 217 (2003) 79.
[45] D. Chen, K.O. Christensen, E. Ochoa-Fernández, Z.X. Yu, B. Tøtdal, N. Latorre, A. Monzón, A. Holmen, J. Catal. 229 (2005) 82.
[46] A.R. Naghash, Z. Xu, T.H. Etsell, Chem. Mater. 17 (2005) 815.
[47] S. Nishimura, Handbook of Heterogeneous Catalytic Hydrogenation for Organic Synthesis, Wiley, New York, 2001.
[48] B. Chen, U. Dingerdissen, J.G.E. Krauter, H.G.J. Lansink Rotgerink, K. Möbus, D.J. Ostgard, P. Panster, T.H. Riermeier, S. Seebald, T. Tacke, H. Trauthwein, Appl. Catal. A 280 (2005) 17.